Hydrogen peroxide modulates lignin and silica deposits in sorghum roots

Nerya Zexer and Rivka Elbaum*

The Robert H. Smith Institute of Plant Sciences and Genetics in Agriculture, The Hebrew University of Jerusalem, 7610001 Rehovot, Israel

One sentence summary: Lignin with carbonyl modifications is patterned by the activity of H_2O_2 to nucleate silica aggregations in sorghum roots.

Author Contribution

Both authors conceived and designed the experiments. N.Z conducted the experiments, and both authors analyzed the data and wrote the manuscript.

The research was funded by the Israeli Ministry of Agriculture & Rural Development, Chief Scientist Office grant 12-01-0016. N.Z is thankful to the Robert H. Smith Foundation for a scholarship.

* Corresponding author: rivka.elbaum@mail.huji.ac.il, +972-8-9489335

Abstract

Silica aggregates in the root endodermis of grasses. Application of Si to roots is associated with variations in the balance of reactive oxygen species (ROS), increased tolerance a broad range of stresses affecting ROS levels, and early lignin deposition. In sorghum (*Sorghum bicolor* L.), silica aggregation is patterned in an active silicification zone (ASZ) by a special type of lignin. Since lignin polymerization is mediated by ROS, we studied the formation of root lignin and silica under varied conditions of ROS and specifically hydrogen peroxide (H_2O_2). Sorghum seedlings were grown hydroponically and supplemented with Si, H_2O_2, and KI. Lignin and silica deposits in the endodermis were studied by optical, scanning electron, and Raman microscopies. Cell wall composition was quantified by thermal gravimetric analysis. We found that silica aggregation was catalyzed by lignin modified by carbonyls. These residues were available for silica nucleation only within 2 hours of their deposition. The endodermal H_2O_2 concentration regulated the intensity but not the pattern of ASZ lignin deposits. Our results show that ASZ lignin is necessary for root silica aggregation in sorghum, and that silicification is enhanced under oxidative stress as a result of increased deposition of the ASZ lignin.

Key words: Active silicification zone; Endodermis ITCW; Hydrogen peroxide; Lignin; Silica aggregates; Silicic acid

Introduction

Silicon oxides are the most abundant mineral group in soils. Therefore, plant roots are always exposed to some silicic acid ($Si(OH)_4$), which is the soluble form of silicates. Addition of silicon to plants is associated with alleviation of varied stresses (Liang *et al.*, 2007; Frew *et al.*, 2018; Coskun *et al.*, 2019*a*). A potent hypothesis explaining the wide-range amelioration of silicon is through variations in the balance of reactive oxygen species (ROS) (Cooke and Leishman, 2016), that play a central role in stress signaling (Choudhury *et al.*, 2017; Prasad *et al.*, 2020). However, we do not know how silicon treatments can affect the oxidative balance. Rice, barley, cucumber and tomato, among other plants, express silicon transporters in their roots (Mitani-Ueno and Ma, 2020). Concerted expression causes super saturation of silicic acid in the xylem sap (Sakurai *et al.*, 2015) of wheat, rice, sorghum and other grasses (Casey *et al.*, 2004; Mitani *et al.*, 2005; Soukup *et al.*, 2020). The silicic acid is transported to the shoot by the transpiration stream and deposited as biogenic opaline silica ($SiO_2 \cdot nH_2O$). This may lead to accumulation of up to 10% silica per tissue dry weight. The deposition takes various mechanisms that are mostly unknown (Hodson, 2016). Heavily silicified locations may be adjacent to cells that are not silicified at all (Lawton, 1980; Bennett, 1982), suggesting a biologically-controlled process. Silica may also form in roots and leaves starved for silicic acid (Kumar *et al.*, 2017; Zexer and Elbaum, 2020), suggesting that biological entities concentrate residual silicic acid to saturation level at the silicification loci. Recently, we reported the first protein that causes silica formation in plants. Siliplant1 (Slp1) is expressed in sorghum (*Sorghum bicolor* L.) epidermis cells called silica cells. It is exported to the cell wall, where it interacts with supersaturated silicic acid solution. Slp1 catalyzes the formation of a thick silica wall within hours (Kumar *et al.*, 2020). In parallel, the cell cytoplasm shrinks into threads, and is eventually evacuated during a programmed cell death (Kumar and Elbaum, 2018).

Silica is also found in sorghum roots, at very specific locations in the cell walls of the endodermis (Sangster and Parry, 1976; Lux *et al.*, 2003; Soukup *et al.*, 2017). However, no Slp1 is expressed in this tissue (Kumar *et al.*, 2020). In contrast to leaves, root silica aggregates on densely deposited lignin with peculiar characteristics (Zexer and Elbaum, 2020). In our previous work we identified an active silicification zone (ASZ) at about 4-8 cm from the root tip (Figure 1). Under silicon starvation, fluorescently green lignin is deposited in the ASZ, forming a spotted pattern on the background of non-modified fluorescently blue lignin. With exposure to silicic acid, this ASZ lignin is silicified, creating the silica aggregation (Zexer and Elbaum, 2020). Endodermal lignification at the Casparian strips is enhanced under Si treatments in comparison to roots starved for silicic acid (Fleck *et al.*, 2011; Lukačová

et al., 2013). This may suggest that in addition to lignin deposition in the Casparian strips, ASZ lignin may also appear earlier under silicic acid treatment.

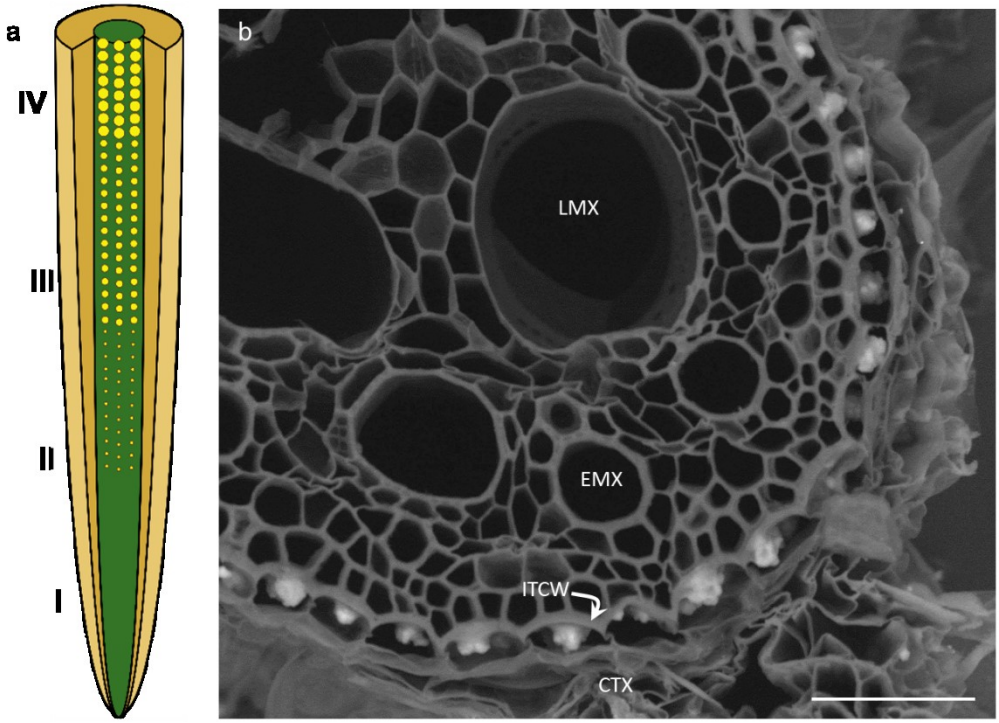

Figure 1. *Silica aggregation along the endodermis of a sorghum (Sorghum bicolor L.) seedling primary root. (a) Schematic diagram of a seminal root, drawn without lateral roots (not to scale). In green we represent the central cylinder and in brown the cortex. The endodermis is a single cell layer that resides between these two tissues. Silica aggregates (yellow circles) develop on the inner tangential cell wall (ITCW) of the endodermis. No aggregates are found at the root tip and up to about 4-6 cm (region I). Aggregation is initiated at about 4-5 cm from the root tip (region II). The aggregates grow in diameter and height along their maturation in regions III and IV. (b) Scanning electron micrograph of a cross section in region IV of a sorghum seedling primary root. The central cylinder shows early (EMX) and late meta-xylem (LMX) vessels. The cortex (CTX) was mostly removed. The thick ITCW (ITCW) is shown with highly bright silica aggregates. Scale bar represents 50 µm.*

Lignin is a polyphenol polymer, which is constructed from monolignols *in situ* at the cell wall. Monolignols are synthesized in the cytosol from phenylalanine and transported to the apoplast, where their polymerization is catalyzed by the activity of peroxidases and laccases. Plant peroxidases are iron containing enzymes that use H_2O_2 to radicalize monolignols. Laccases are multi-copper oxidase glycoproteins that catalyze monolignols oxidation by reducing molecular oxygen to water. The activity

83 of both enzymes results in monolignol radicals free to react with the growing lignin polymer (Wang *et*
84 *al.*, 2013; Meents *et al.*, 2018). Formation of local deposits of lignin is achieved by the localized binding
85 of laccases and peroxidases complexes to the cell wall (Lee *et al.*, 2013; Schuetz *et al.*, 2014; Hoffmann
86 *et al.*, 2020). Under the hypotheses of this mechanism, lignin will be formed from the monomers available
87 in the vicinity of the bound enzymes. Several models aiming to explain cellular export of monolignol
88 have been hypothesized. Namely, by vesicle-mediated exocytosis, via activity of membrane localized
89 transporters, and passive diffusion through the cell membrane (Dixon and Barros, 2019). However, while
90 lignification is undoubtedly a tightly regulated process in both space and time, there is currently no clear
91 evidence for the directed and localized secretion of lignin building blocks (Meents *et al.*, 2018), and
92 specifically, patterning of modified lignin that can explain the ASZ lignin formation on the background
93 of non-modified lignin.
94 Therefore, in this work we explored the effect of H_2O_2 variation on silica and lignin formation in roots
95 of sorghum seedling. We show that the deposition of ASZ lignin is not advanced to younger tissues with
96 Si treatments and that its binding in the endodermis cell wall is possible only through the activity of
97 H_2O_2, suggesting its polymerization by peroxidases.
98
99 **Results**
100 In order to examine ROS influence on silica aggregation in seminal roots of sorghum seedlings, we first
101 aimed to increase their endogenous concentration by applying injury, salt and oxidative stress. Roots of
102 Si- seedlings were poked with a syringe needle, after which the plants were transferred to Si+ hydroponic
103 media for recovery. After 3 days, no aggregates formed at the injury location, possibly due to tissue
104 damage and cell death. Adjacent to the injury, the average footprint of the silica aggregates on the
105 endodermis inner tangential cell wall (ITCW) was larger in relation to aggregates that developed in
106 parallel regions of uninjured roots (Figure 2). Roots were subjected to salinity and H_2O_2 stresses by
107 transferring Si- seedlings to Si+ hydroponics media supplemented with 50 mM NaCl or increasing
108 concentration of H_2O_2. In these roots, too, we found larger silica aggregates compared to non-stressed
109 roots (Figure 3). Interestingly, the increase in projected area was negatively correlated to the H_2O_2
110 concentration.

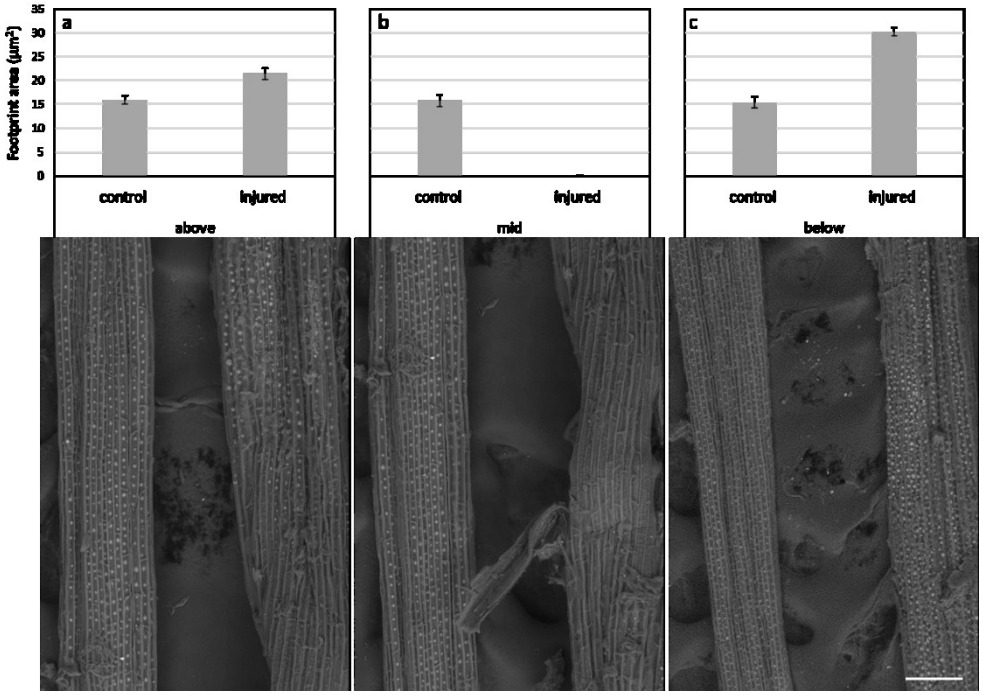

Figure 2. *The effect of local injury on silica aggregates footprint. Bottom panels show scanning electron micrographs of an uninjured root (left) and a root locally injured using a needle (right). Above each micrograph is a graph of the measured mean footprint of the aggregates. Bars represent standard error. Variations between the treatments are statistically significant. (a) In the region about 0.5 mm above the injury, the aggregates that formed in the injured root were larger than aggregates in the uninjured root. (b) No aggregates were found around the injured area. (c) In the region about 0.5 mm below the site of injury, the aggregates that formed in the injured root were larger than aggregates in the uninjured root. Scale bar in panel c, common to all micrographs, represents 100 µm.*

Figure 3. *The effect of exogenous H_2O_2 and NaCl treatments on the average footprint of root silica aggregates in the endodermal ITCW. Presented are mean aggregate areas and standard errors. Treatment of 10 mM H_2O_2 resulted in an aggregate footprint 15% larger than aggregates in unstressed (control) roots. Similar increase was measured under 50 mM NaCl stress. Bars represent standard errors and different letters indicate significant differences at $p \leq 0.05$.*

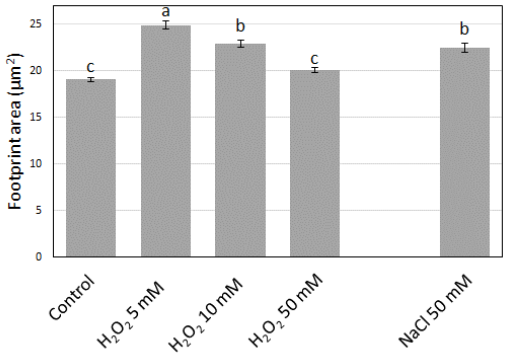

130 *Initiation of silica and lignin patterns are influenced similarly by ROS balance*

131 Our results suggested that silica aggregation increases under moderate increase of the oxidative state of
132 roots. To identify the root region in which ROS affected silica aggregation, we monitored silica formation
133 along the root maturation gradient, comparing region I to regions II-III (Figure 1) under varied oxidative
134 levels. For this, seedlings were grown for 3 days in Si- hydroponics solution, allowing a mature non-
135 silicified tissue to develop. On the 4th day, the seedlings were transferred to Si+ hydroponics solution
136 supplemented with 5 mM H_2O_2 for additional 3 days. This allowed a younger part of the root to develop
137 under oxidative stress and silicic acid. In another treatment, 1 mM KI was added, which quenched
138 physiological H_2O_2, reducing the native ROS concentration. We then tested these roots for silica
139 aggregate formation in three regions: (1) young developing tissue about 1 cm from the root tip,
140 developing under altered ROS balance (region I), (2) mature region composed of cells that were exposed
141 to silicic acid in parallel to completing their maturation under high/low ROS concentrations (region III),
142 and (3) mature region, containing cells that were exposed to silicic acid only after completing their
143 development under benign conditions (region IV). H_2O_2 treatment considerably stunted root growth,
144 while under KI treatment the average length of the roots was similar to that of untreated samples (Figure
145 4a-c). In the mature part of the roots (region IV), the silica deposition was similar between all treatments
146 (Figure 4d-f). However, silica aggregation was detected already in region I under H_2O_2, and only in
147 region IV under KI (Figure 5f-l). Our results suggested that developmental processes in the young root
148 that respond to the altered ROS levels affected silica aggregation. Such a process may presumably be
149 lignin deposition.
150

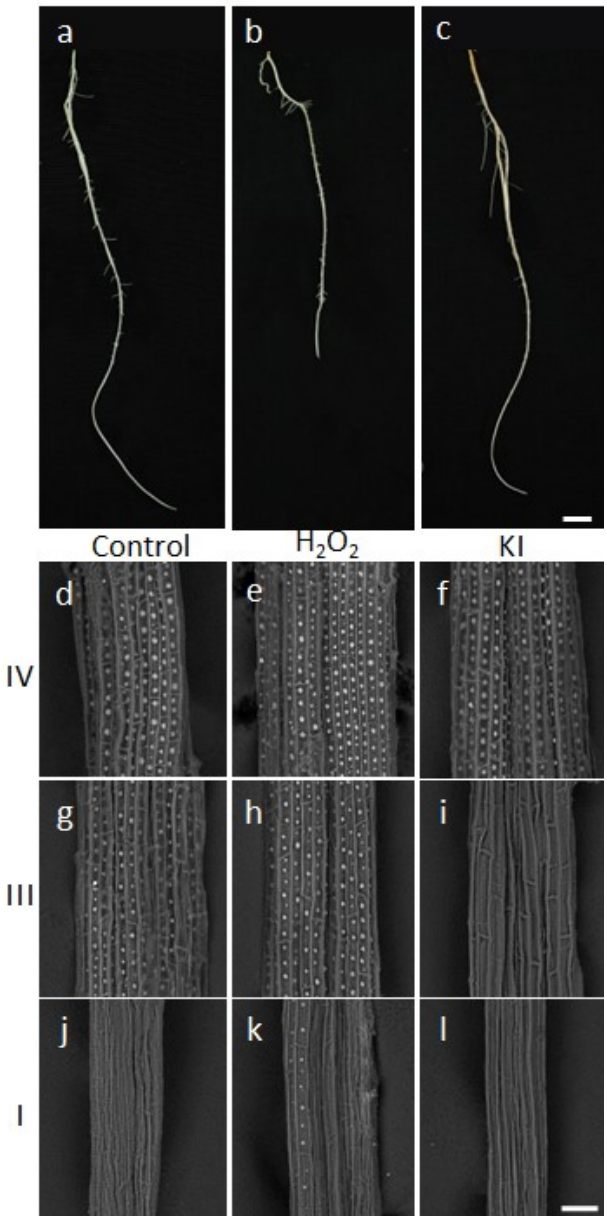

Figure 4. *Silica deposition in the endodermal ITCW under high and low H_2O_2 regimes. Roots grown in Si- media for three days were transferred to Si+ (control), Si+ & 5 mM H_2O_2, and Si+ & 1 mM KI treatment media for additional four days. (a-c) Representative images of (a) control, (b) H_2O_2, and (c) KI treated roots. (d-f) Scanning electron micrographs of region IV of (d) control roots, and (e) H_2O_2, and (f) KI treated roots. (g-i) Scanning electron micrographs of region III of (g) control roots, and (h) H_2O_2, and (i) KI treated roots. (j-l) Scanning electron micrographs of region I of (j) control roots, and (k) H_2O_2, and (l) KI treated roots. In roots treated with H_2O_2, silica aggregates formed prematurely in region I. No aggregates developed in cells that completed their development under KI treatment. Scale bar in c, common to a-c, represents 1 cm. Scale bar in panel l, common to d-l, represents 50 µm.*

In order to follow the formation of the lignin spots in the endodermis, 6 days old roots grown under Si+ and Si- treatments were stained for lignin by phloroglucinol-HCl (Figure 5). In the Si+ roots, the ITCW exhibited spots of staining intensity lower than the staining of the background ITCW, possibly indicating silica aggregation. In the Si- treatment, spots of increased staining were patterned similarly (Figure 5a-f). We then examined 6-days old Si- roots that were grown for 3 days under H_2O_2 or KI treatments. The phloroglucinol-HCl staining behaved similarly to the silica aggregation pattern revealed in Figure 4: Under H_2O_2 treatment spots initiated in region I, and under KI treatment spots were found only in region IV (Figure 5g-l).

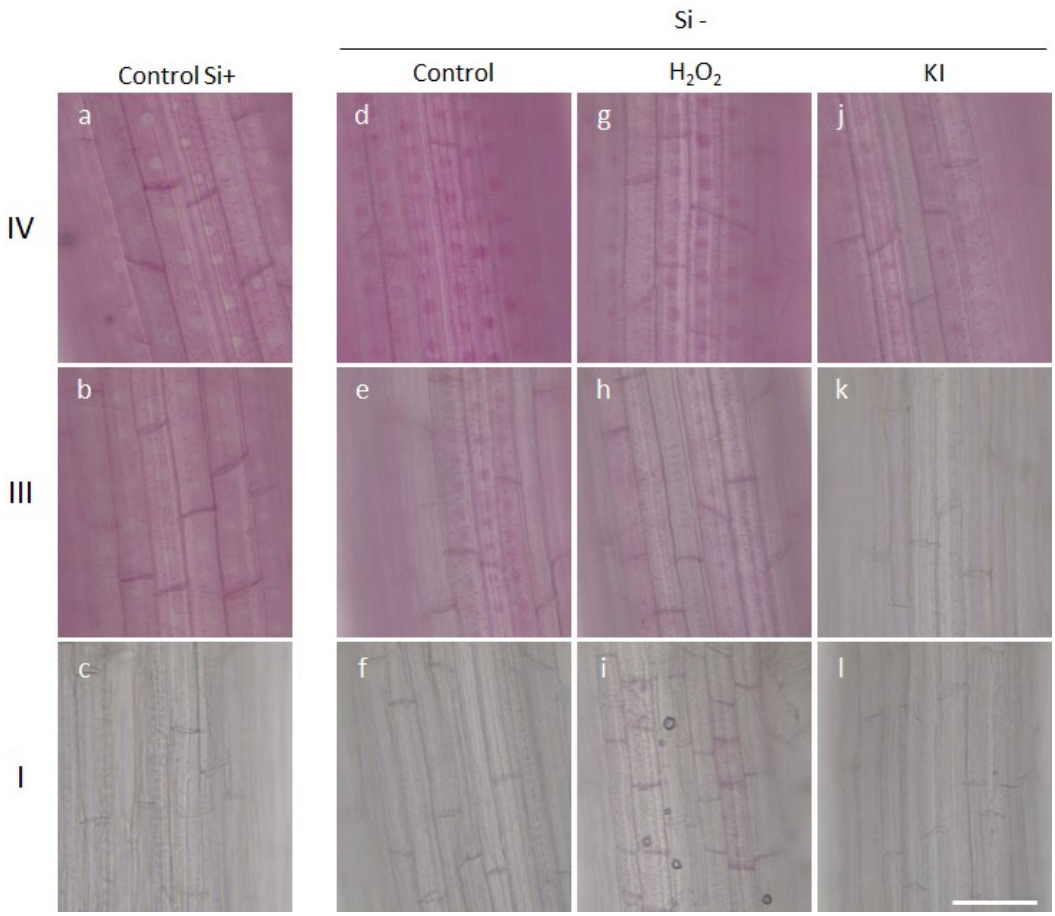

182 ***Figure 5.*** *Lignin deposition in the endodermal ITCW under high and low H_2O_2 regimes. (a-c) Roots*
183 *grown in Si- media for three days were transferred to Si+ media and stained for lignin with*
184 *Phloroglucinol-HCl. Unstained silica aggregates are evident on the stained background of the ITCW in*
185 *regions IV (a) and III (b). (c) There is no staining in region I. (d-l) Roots grown in Si- media for three*
186 *days were transferred to Si- (control), Si- & 5 mM H_2O_2, and Si- & 1 mM KI treatment media for an*
187 *additional four days and stained for lignin with Phloroglucinol-HCl. Optical micrographs were collected*
188 *from control (d-f), H_2O_2 (g-i) and KI (j-l) treatments, in region IV (top panels), III (middle panels), and*
189 *I (bottom panels). In roots treated with H_2O_2, deposits of lignin in spots formed prematurely in region I.*
190 *Lignin spots are not detected in cells that completed their development under KI treatment. Scale bar in*
191 *l, common to all panels represents 50 µm.*
192
193 *ASZ lignin formation and silica aggregation are not advanced by silicic acid treatment*
194 Quantitative comparison of the patterns of Si+ and Si- roots was achieved by autofluorescence
195 microscopy, showing silica aggregation in blue (Soukup *et al.*, 2014) and ASZ lignin in green (Zexer and
196 Elbaum, 2020). The distance from the root tip to the first blue (Si+) or green (Si-) spot was measured

197 under H_2O_2 or KI treatments (Figure 6). Under all ROS regimes, the average distance to the first
198 fluorescent spot was similar between Si+ and Si- treatment. We therefore concluded that the aggregates
199 in Si+ and the lignin spots in Si- roots represent the same oxidative phenomenon in the same locations
200 and developmental stage.
201
202
203 ***Figure 6.*** *Location along the root of initial silica*
204 *aggregation (in Si+ roots) or lignin spotted pattern*
205 *(in Si- roots). The average distance from the root tip*
206 *to the first auto fluorescent spot is plotted in control,*
207 *H_2O_2, and KI treated roots. Bars represent standard*
208 *error. Different letters indicate significant*
209 *differences at $p \leq 0.05$.*

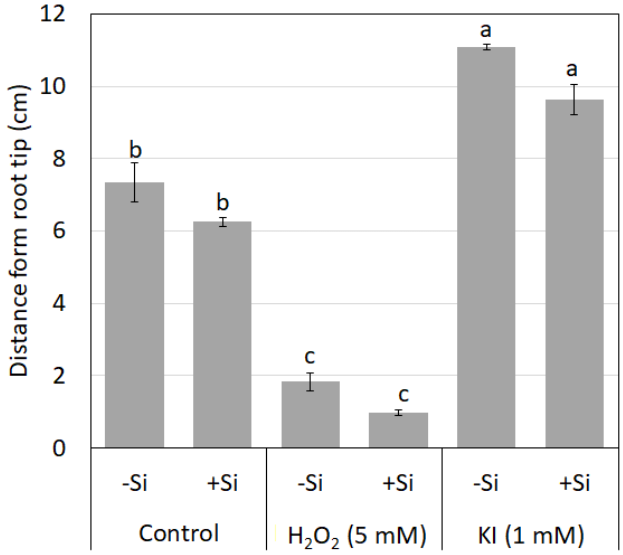

210
211
212 To further study the influence of silicic acid on ASZ lignin and silica deposition, we stained roots grown
213 with (Si+) and without (Si-) silicic acid by 3,3′-diaminobenzidine (DAB) (Figure 7). DAB is oxidized in
214 the presence of H_2O_2 and heme-containing enzymes. As a result, dark precipitates form in stained tissues
215 (Daudi and O'Brien, 2012). Since laccases lack the ability to oxidize DAB, this staining method can be
216 viewed as an indicator for peroxidases activity (Barceló, 1995). Brown staining was identified in region
217 II, where silica aggregation is initiated (Figure 1). A continuum of brown discoloration formed from the
218 endodermal inner tangential cell wall (ITCW) to the nearest metaxylem element. The staining along the
219 roots was similar between Si- and Si+ treatments (Figure 7a-f). Our results suggest that ASZ lignin
220 formation is facilitated by H_2O_2 and is not advanced under Si treatment. Nonetheless, under Si- treatment
221 the ITCW innermost layer in region III revealed a pattern of darker DAB-stained spots (Figure 7g). In
222 the same region under Si+ treatment, we detected dark rings on a uniformly DAB-stained background
223 ITCW (Figure 7h). Both spots and rings, which indicated high peroxidase activity, formed a pattern
224 similar to that of silica aggregation.

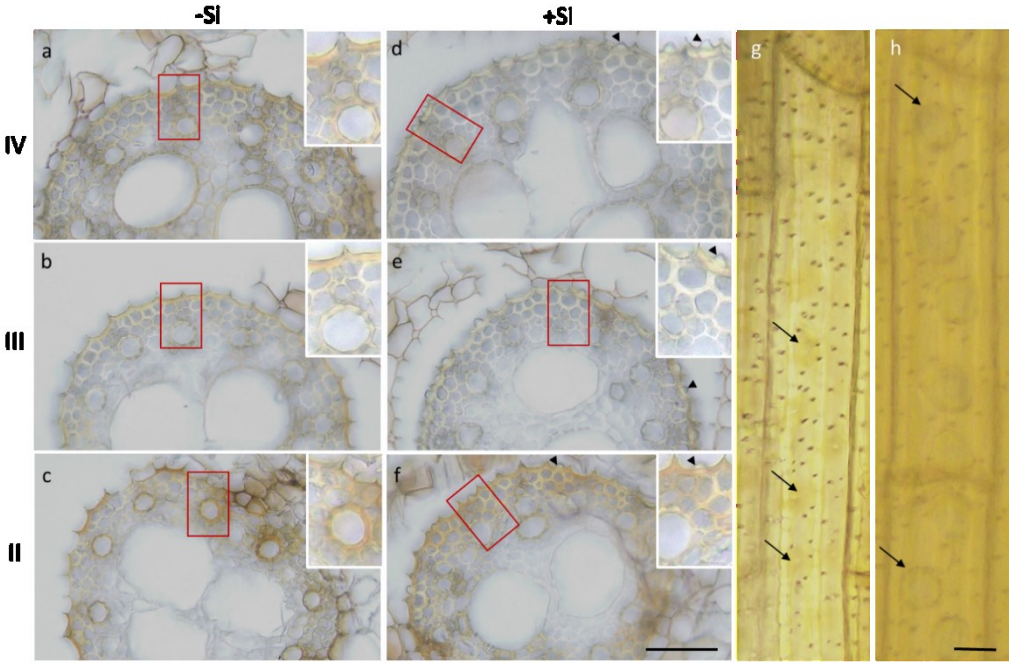

Figure 7. *Primary roots of sorghum seedlings stained with 3,3'-diaminobenzidine (DAB). Cross sections taken from a Si- (a-c) and a Si+ root (d-f) represent regions IV, III, and II of silica aggregation along the root, as defined in Figure 1. Insets are enlargements of the red rectangles in each of the panels. Brown discoloration attributed to the precipitation of DAB can be seen in the endodermal ITCW and the cell walls of xylem elements in all three regions. The staining is more intense in region II of both treatments. This is the region of Si aggregation onset. Arrowheads indicate some silica aggregates. (g) A longitudinal view of DAB stained ITCW from a Si- root. Slightly stronger tainted spots (arrows) can be seen on the background of the stained cell wall. Pits are seen as dark dots. (h) A similar longitudinal view of a Si+ ITCW. The outlines of Si aggregates are evident in darker stain (arrows) on the uniformly stained ITCW. Scale bar in f, common to a-f represents 50 µm. Scale bar in h, d common to g and h represents 5 µm.*

KI treatment depressed lignin spotted pattern but not general lignin deposition

The variation in oxidative state of the roots that affected the silica deposition most likely also affected the cell wall composition. The H_2O_2 treatments stunted the roots (Figure 2b), indicating their effects on many developmental processes. We therefore analyzed the cell walls of Si- roots grown under KI treatment that did not affect root visual phenotypes (Figure 2c). Thermal gravimetric analysis (TGA) is a sensitive method for quantifying cell wall composition (Abidi *et al.*, 2008; Abraham *et al.*, 2018). Analysis of 30 roots in 3 bulk samples revealed four decomposition peaks, assigned to lignin, cellulose, and hemicellulose (Figure 8) (Yang *et al.*, 2007). The lignin decomposition temperature was similar

245 between the treatments, at 434 ± 44°C. The cellulose decomposed in two stages, at 311 ± 3°C and 323 ±
246 2°C, similarly in both treated and non-treated samples. However, in KI treated roots the hemicellulose
247 decomposed at a lower temperature (266.5 ± 0.3°C) than the non-treated roots (283 ± 4°C). Variations in
248 the weight fractions of these three main cell wall components were non-significant at 5% level (Table 1).
249
250
251
252 ***Figure 8.*** *Differential thermal gravimetric analysis of*
253 *Si- roots grown under control (black) or 1 mM KI*
254 *(gray) treatment. Three biological repetitions of 30*
255 *peeled roots were measured for each treatment.*

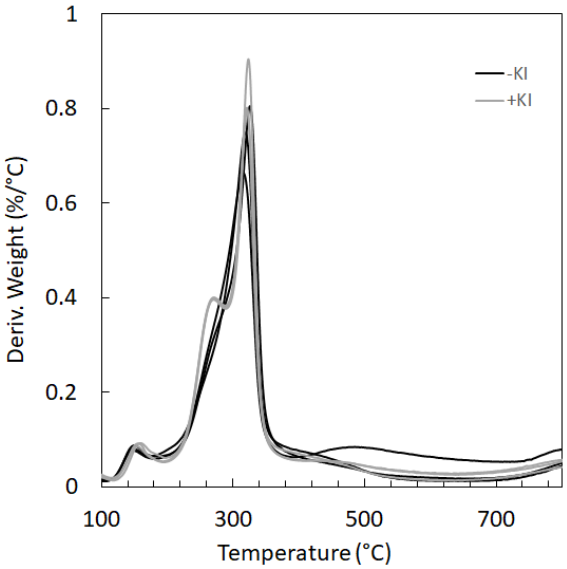

256
257
258
259
260
261 ***Table 1.*** *Composition of the cell walls of peeled seedling's roots based on TGA. The average weight*
262 *percent and standard deviation of hemicellulose, cellulose, and lignin was calculated by peak fitting to*
263 *the differential weight percent at about 266 - 283°C (hemicellulose), 311 - 323°C (cellulose), and 390 -*
264 *480°C (lignin). Averages of 3 samples each containing 30 roots is reported.*

	hemicellulose	***cellulose***	***lignin***
KI-	*44 ± 11*	*49 ± 13*	*7 ± 2*
KI+	*32.6 ± 0.8*	*64 ± 1*	*3 ± 2*
P (T-test)	*0.23*	*0.19*	*0.09*

265
266 Raman micro-spectroscopy was used to monitor lignin composition and distribution (Figure 9). Average
267 spectra of whole Raman maps showed typical lignocellulosic trace, with major cellulose peaks at 378,
268 1095 cm^{-1}, and lignin at 1171, 1600, 1630, 1660 cm^{-1} (Agarwal and Ralph, 1997; Agarwal, 2014). The
269 KI treated sample average spectrum showed smaller scatterings of lignin at 1171, 1200 cm^{-1} than the
270 control spectrum (Figure 9a). Spectral first derivative enhanced hidden peaks and reduced fluorescence
271 background. Derivation of the aromatics doublet at 1600-1630 cm^{-1} revealed peak shoulders at 1585 and

1660 cm^{-1} only in the non-treated control roots (Figure 9b,c). The 1585 cm^{-1} shoulder was assigned to lignin in sugarcane (Agarwal, 2014), and the 1660 cm^{-1} to lignin in black spruce (Agarwal and Ralph, 1997). Mapping the total Raman signal in non-treated roots revealed a spotted pattern, suggesting that the cell wall in these locations is denser than their surroundings (Figure 9d). This is in accordance with our published finding of higher intensity of SEM back scattered electrons at the spots, relative to the surrounding cell wall (Zexer and Elbaum, 2020). In the KI treated samples, no spots were identified, suggesting that dense cell wall did not develop (Figure 9e).

In order to identify specific Raman peaks related to the spots while compensating for the general higher signal, we mapped lignin peaks normalized to the crystalline cellulose peak at 378 cm^{-1} (Figure 9f-k).

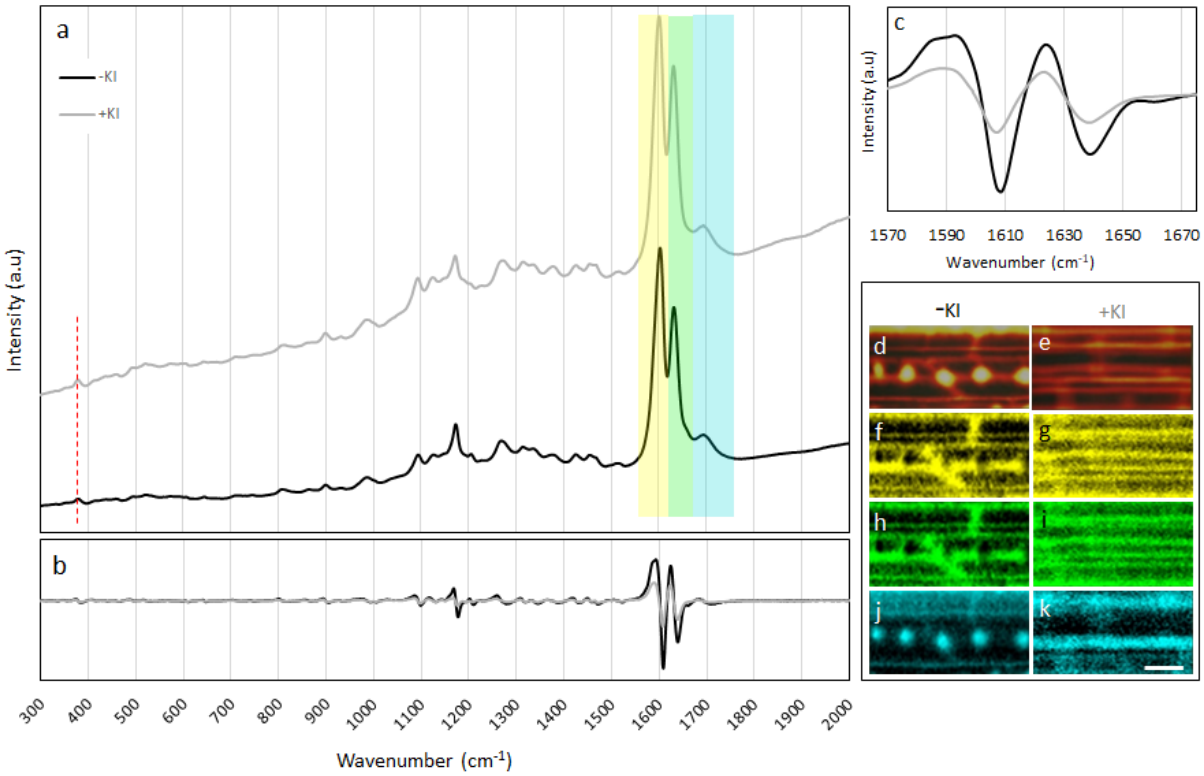

Figure 9. *Raman micro-spectroscopy of endodermal ITCW in Si- roots grown under control or KI (1 mM) treatment. (a) Average spectra of ITCW maps of control (black) and KI (gray) treated roots. The colored rectangles indicate spectral regions mapped in panels f-k, normalized to the crystalline cellulose peak at 378 cm^{-1} (red dashed line). (b) First derivative of the average spectra in panel A. (c) Enlargement of the spectral range 1570-1675 cm^{-1} in panel B. (d-e) Maps of the total Raman signal measured from the ITCW of (d) control and (e) KI treated roots. (f-k) Maps depicting typical lignin signals normalized to the crystalline cellulose peak at 378 cm^{-1} of control (left) and KI (right) treated roots. (f-g, yellow)*

1550-1618 cm^{-1}, (h-i, green) 1618-1660 cm^{-1}, (j-k, cyan) 1660-1750 cm^{-1}. Scale bar in k, common to d-k, represents 20 µm.

Interestingly, the aromatic signal at 1660-1750 cm^{-1} was enriched in the spots (Figure 9j), and so was the 1660 cm^{-1} shoulder. This spectral region may indicate the presence of aromatic carbonyls (Agarwal and Ralph, 1997; Taylor and Zografi, 1997). In contrast, the relative intensity of the major lignin doublet at 1590-1610 cm^{-1} and 1620-1630 cm^{-1} did not illuminate the spots (Figure 9f,h), and neither the shoulder at 1585 cm^{-1}. This indicates that generally, lignin is distributed evenly in the endodermis ITCW, however, the aromatic carbonyl groups are enriched in a spotted pattern. In the roots treated with KI, we could not detect the spotted pattern by any mapping strategy (Figure 9e,g,i,k).

The incorporation of carbonyl residues into lignin is increased under reduced activity of cinnamyl alcohol dehydrogenase (CAD), (Stewart *et al.*, 1997). Similarly, a mutation in CAD that causes a brown mid-rib phenotype in the *Sorghum bicolor* mutant *bmr6* (Sattler *et al.*, 2009), possibly increases the fraction of carbonyl aldehydes in the lignin (Yahiaoui *et al.*, 1997). Interestingly, in roots of sorghum *bmr6* mutant on the background of line BTx623, the average silica aggregate footprint was larger by 70% than that in the wild type BTx623. We measured mean footprints (± SE) of 24 ± 5 µm^2 in the wild-type plants and 39 ± 9 µm^2 in the *bmr6* mutant plants, significantly different between the genotypes. Our results strongly indicate that the ASZ lignin is enriched with carbonyl groups conjugated to aromatic rings. These modifications may nucleate silicic acid in the roots of sorghum.

Lignin active deposition is required for the silica to aggregate

Aiming to test whether the ASZ lignin spots are required for the formation of silica aggregation, we exposed roots treated by KI to silicic acid. Three exposure schemes were compared: (1) Sorghum seedlings were grown for 1 week under Si- solution. After 1 week, the seedlings were pretreated for 2 hours with Si- & KI solution, and then moved to Si+ & KI for an additional 12 hours. (2) Seedlings were grown under Si- & KI solution for 1 week, and then moved to Si+ & KI for 12 hours. (3) As a control, we grew seedlings in Si- solution, which were transferred after 1 week into Si+ for 12 hours (no KI was applied). In our hydroponics system, the basal 1 cm of the roots, closest to the root-shoot junction, was surrounded by a polystyrene foam plate that supported the seedlings. Therefore, this region of the roots was not exposed to the growing medium but to air. We monitored silica aggregation in mature root tissues, below and above the hydroponics solution (Figure 10).

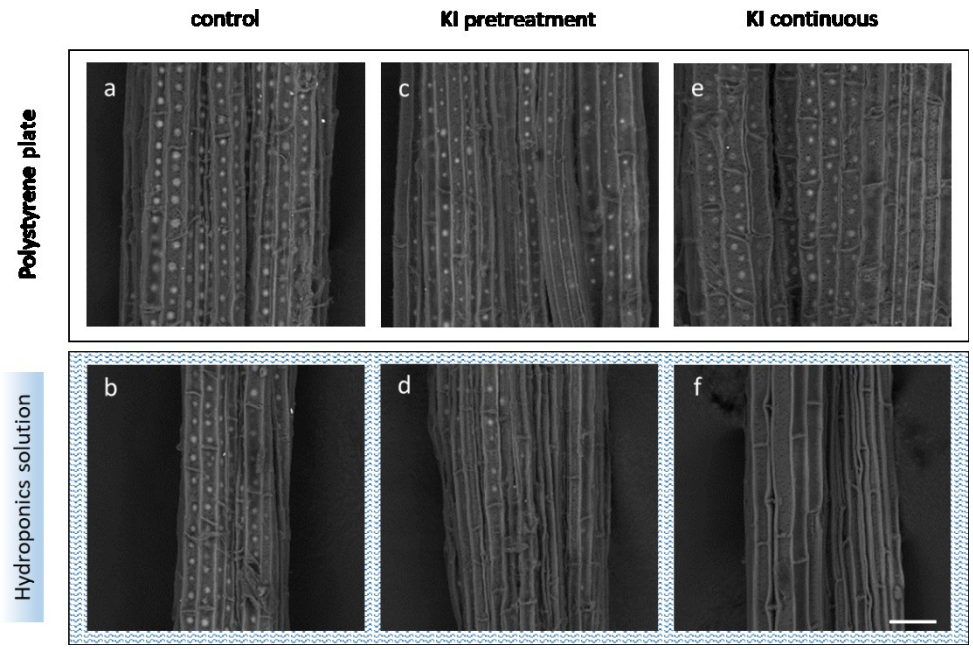

Figure 10. *The effect of KI 2-hour pretreatment and KI continuous treatment on the formation of silica aggregates, depicted by scanning electron microscopy. (a,b) Roots were grown under Si- for 3 days and then moved to Si+ medium for another 3 days (control). (c,d) Roots grown in Si- solution were pretreated by KI and then moved to Si+ & KI for another 3 days (KI pretreatment). (e,f) Roots grown in Si- solution were moved to Si+ & KI treatment for another 3 days (KI continuous). (a,c,e) Micrographs of root sections from the basal end. This root part was not in contact with the hydroponics solutions. (b,d,f) Micrographs of mature root tissues in region IV that were immersed in the hydroponics solutions. Scale bar in f, common to all panels, represents 50 µm.*

In the basal root part, never exposed to KI solution, silica aggregates developed regardless the treatment (Figure 10a,c,e). In the immersed parts of the root, the formation of aggregates under KI pretreatment was dramatically hindered compared to control roots (Figure 10b,d). Importantly, in this region, the ASZ lignin spotted pattern was fully developed, similarly to that in Si- roots. In roots cultivated with KI the entire growing period, aggregates were missing altogether (Figure 10f). Collectively, our results suggest that deposition of ASZ lignin in spotted pattern is activated by apoplastic H_2O_2 and that silica aggregates onto these spots only a short time after their formation.

Discussion

Silica deposits require an optimal level of H_2O_2

337 In sorghum roots, silica aggregates are deposited in a neatly ordered pattern as part of the endodermal
338 ITCW. This process is only attained by live tissue and is metabolically controlled (Soukup *et al.*, 2020).
339 Damaging the root locally prevented the formation of aggregates next to the wound, possibly as a result
340 of cell death at the endodermis (Figure 2). Our results showed that excess H_2O_2 concentration is
341 negatively correlated to the aggregate footprint, with highest effect at the lowest concentration tested
342 (Figure 3). Aggregates were bigger below the wound, as compared to above it (Figure 2). As the
343 apoplastic H_2O_2 moves up the root with the transpiration stream, this trend may also reflect a stronger
344 effect of a small increase in H_2O_2 concentrations. The complex relationship between ROS balance and
345 silica deposition is in accord with the dual role of ROS in redox biology, that at low concentration induces
346 cell proliferation, differentiation and elongation, and at high concentration signals for stress and cell
347 death, and may apply stress via oxidation of useful molecules (Tsukagoshi *et al.*, 2010; Schieber and
348 Chandel, 2014). Nonetheless, under very low endogenic H_2O_2 concentration, during KI treatments,
349 aggregates did not form (Figure 4,10). Since the tissue still contained lignin (Figure 6,8,9), it appears that
350 the general deposition of lignin occurred also under a minimal level of H_2O_2. However, ASZ lignin
351 patterning of the silica aggregation sites requires a higher H_2O_2 level.

352 *Low H_2O_2 concentration reduces hemicellulose cross-linkage*

353 Under KI treatments, the hemicellulose pyrolysis temperature was lower by 16°C (266.5 ± 0.3°C in
354 treated roots and 283 ± 4°C in non-treated roots). Such a decrease in thermal stability may be a result of
355 reduced levels of cross-linking (Farhat *et al.*, 2017). Hemicellulose polymers are cross-linked to one
356 another through di-ferulic acid ester bonds and to lignin by ester or ether bonds of ferulic or coumaric
357 acid (Hatfield *et al.*, 2017). In maize cell culture, exogenous H_2O_2 treatment leads to increased cross-
358 linkage of the hemicellulose by ferulic acid, monolignols, and other phenylpropanoids (Fry *et al.*, 2000).
359 Further, the random nature of these bonds may increase the variability of hemicellulose pyrolysis
360 temperature, which is 10 times higher in the control samples as compared to the samples grown under
361 KI. In contrast, the pyrolysis of lignin was similar between the treatments, suggesting that lignin cross-
362 linkage was not altered (Stewart *et al.*, 1997).

363 *Silica deposits on lignin that is polymerized in reaction to H_2O_2 activity*

364 The lignin spotted pattern developed in plants starved for silicic acid, similarly to the silica aggregation
365 pattern in plants fed with silicic acid (Figure 6). The two phenomena co-localize, as the fluorescently
366 green lignin spots overlap the Raman spotted pattern and the SEM spots of dense cell wall that nucleates
367 silica (Zexer and Elbaum, 2020). Our results show that the ASZ lignin deposition was independent of
368 silicic acid. In contrast, in roots treated by KI, no ASZ lignin nor silica deposited. A hierarchical

369 relationship appears, in which H_2O_2 is required for the formation of lignin that is needed for silica
370 aggregation.
371 When the formation of lignin was arrested concurrently with the application of silicic acid, normal silica
372 aggregation occurred in region IV (Figure 4f). This suggests that the tissue was ready for the nucleation
373 of silicic acid before the arresting of lignin formation. In contrast, the similar root region under similar
374 growing conditions did not nucleate silicic acid when it was pretreated with KI for 2 hours (Figure 10d).
375 This result indicates that the spots of ASZ lignin, deposited before the KI treatment, were not active in
376 nucleating the silicic acid, and implies that the ASZ lignin can nucleate silica aggregation only during a
377 short window of time after its deposition. Further, once silica had started to form, the aggregate continued
378 to grow independently of the lignin polymerization (Figure 4f).
379 *ASZ lignin patterning*
380 Lignin formation requires a source for radicals. These could be oxygen molecules processed
381 enzymatically by laccases. Alternatively, NADPH oxidase (called respiratory burst oxidase homologs
382 (RBOH) in plants) produces $O_2^{-\cdot}$ that are converted to H_2O_2 molecules, processed by peroxidases. A
383 radical is transferred by the enzymes to a phenylpropanoid, which is coupled to a growing lignin polymer.
384 In Arabidopsis, lignin deposition is patterned by the formation of enzyme complexes bound to the cell
385 wall under specific developmental contexts, such as lignification of root Casperian strips or xylem
386 elements (Lee *et al.*, 2013; Hoffmann *et al.*, 2020). The enzyme complexes include anchoring motifs,
387 RBOHs, superoxide dismutase (SOD), and laccases or peroxidases. In our system, we find profound
388 influence of apoplastic H_2O_2 concentration on the intensity of localized lignification. This suggests the
389 involvement of peroxidases in the formation of the ASZ lignin spots in the tertiary cell wall.
390 Nonetheless, the pattern of lignification was not altered under the H_2O_2 treatments, suggesting that the
391 endogenous production of H_2O_2 does not control the lignin patterning. Therefore, the pattern could
392 originate from a pattern of peroxidases bound to the cell wall, or by modified monolignols (typical to
393 ASZ lignin) that are in some way bound specifically in spots. Lignification occurs over the whole surface
394 of the tertiary cell wall, with lower deposition in the spots, as seen by mapping the Raman total lignin
395 scattering (Figure 9d,e). This suggests the activity of peroxidases and / or laccases throughout the ITCW.
396 Since total lignin formation was only slightly reduced by KI treatment (Table 1), we may assume that
397 the lignin forming in the seedling root is mostly produced as a result of laccases activity, unaffected by
398 low levels of H_2O_2. This may suggest that the ASZ lignin pattern forms by patterning of peroxidases on
399 a background of laccases. However, both laccases and peroxidases will interact with whatever lignin
400 monomers they may find, including the ASZ lignin monomers. Therefore, our results suggest that the

401 spotted pattern of modified lignin either originated from patterned ASZ-phenylpropanoid monomers or
402 required the involvement of dirigent proteins that selectively interact with specific monolignols (Dixon
403 and Barros, 2019; Tobimatsu and Schuetz, 2019). Another option could be the oxidation of the lignin to
404 produce carbonyls modifications *in situ* at the spot location. However, no experimental evidence supports
405 this modification mechanism (Dixon and Barros, 2019). Since monolignols diffuse freely in the cell wall,
406 the binding of modified ASZ lignin monomers must be very rapid. Only the freshly added lignin moieties
407 interacted with silicic acid molecules and nucleated a silica aggregate. When silicic acid was not
408 available, peroxidase activity formed spots at the endodermis ITCW (Figure 7g), possibly cross linking
409 the ASZ lignin monomers to form a dense cell wall (Figure 9d). Once cross-linked, the ASZ lignin is
410 unavailable for aggregating the silica.

411 *Silicon, H_2O_2 and lignin crosstalk*

412 Silicon in plants is studied as a stress-ameliorating agent. Reports encompass species from diverse plant
413 families confronting a range of both biotic and abiotic stresses (Liang *et al.*, 2007; Van Bockhaven *et al.*,
414 2013; Coskun *et al.*, 2019*b*). Many of these works point to Si-generated effects on plants' oxidative state
415 including gene regulation, protein abundance and ROS levels (reviewed by Cooke and Leishman, 2016).
416 A specific example in root endodermis shows that the supplementation of silicic acid to the growing
417 medium enhances lignification (Fleck *et al.*, 2011; Lukačová *et al.*, 2013) but not suberization (Kreszies
418 *et al.*, 2020) through modulation of ROS and ROS-dependent enzymes (Fleck *et al.*, 2011). In this work,
419 we show a reciprocal effect: The apoplastic oxidative levels affect the extent of endodermal silicification
420 in roots of sorghum seedlings through mediation of lignin formation. This new direction requires further
421 work to show whether it links to stress signaling.

422

423 **Materials and Methods**

424 *Plant material and growth conditions*

425 Grains of *Sorghum bicolor* (L.) Moench, line BTx623 and BTx623 *bmr6* mutants were surface sterilized
426 with 3% sodium hypochlorite for 10 min and rinsed twice with distilled water. The *bmr6* genetic stock
427 is PI639713, obtained from the USDA. Grains were then placed in petri dishes lined with wet filter papers
428 and germinated for 72 h. After germination, seedlings were grown hydroponically for one week. All
429 growth solutions were based on double distilled water containing 1 mM $CaCl_2$. Si+ medium was
430 supplemented with sodium silicate (Na_2SiO_3) at a final concentration of 2 mM. Si- medium was
431 supplemented with NaCl at a similar final concentration in order to maintain equal ionic balance across
432 all media. The final pH of all the solutions was adjusted to 5.8 with HCl. In relevant experiments, NaCl,

433 KI and H_2O_2 (Sigma-Aldrich) were added to the solutions. Seedling were grown on plates of polystyrene
434 foam mounted on top darkened 1 L beakers containing growing media. In each beaker we grew ten
435 seedlings. Cultivation was done in a growth chamber, under controlled conditions with photoperiod 16
436 h : 8 h (light : dark) illuminated with photosynthetic active radiation (PAR) of approximately 200 µmol
437 m^{-2} s^{-1}, at a temperature of 28°C : 22°C (light : dark), and 70% air humidity.
438 *Root tissue fixation*
439 Complete primary roots were harvested and fixed in ethanol : acetic acid (9:1 v/v) under vacuum for 24
440 hours. Root samples were kept in the same fixative at 4°C for additional 48 hours. The fixing solution
441 was then replaced with ethanol 70% and samples were stored at 4°C until use.
442 *3,3'-diaminobenzidine (DAB) staining and roots sectioning*
443 DAB staining was preformed according to Daudi & O'Brien (2012) with minor changes. Briefly,
444 complete excised primary roots were immersed in petri dishes containing freshly made DAB aqueous
445 solution (5.2 mM, Sigma-Aldrich). Appropriate infiltration of the stain was ensured by applying gentle
446 vacuum for 5 min using a desiccator. Petri dishes were then covered with aluminum foil and placed on a
447 laboratory shaker. After 5 hours of gentle shaking, root samples were transferred to ethanol : acetic acid
448 (9:1 v/v) fixative solution. The solution was replaced once and followed by the fixation procedure
449 described earlier.
450 Three-millimeter-long root sections were rinsed with double distilled water, positioned in plastic molds,
451 and embedded in O.C.T embedding compound (Scigen, USA). The molds were carefully lowered into
452 liquid nitrogen until the O.C.T medium froze. A CM1860 cryostat (Leica) was used to cut 20 µm thick
453 sections, which were mounted on glass slides. These were observed and photographed with a Leica
454 DM500 microscope equipped with an x40 objective and coupled to a Leica ICC50W camera.
455 *Aggregate assessments by scanning electron microscopy (SEM)*
456 Fixed root samples were carefully peeled out of their cortical tissues using finely serrated tweezers.
457 Representative segments of each sample were mounted on aluminum stubs using carbon tape.
458 Observations were performed with a JEOL JSM-IT 100 InTouchScope™ scanning electron microscope
459 (SEM), (JEOL, Japan) under low vacuum (30 Pa) and with accelerating voltage of 20 kV. All
460 micrographs were taken using the back scattered electrons mode. Aggregates footprint were measured
461 by analysis of the SEM micrographs using ImageJ2 software (Schneider *et al.*, 2012).
462 *Phloroglucinol-HCL staining*
463 Staining solution was prepared by mixing a 3% Phloroglucinol (Sigma-Aldrich) solution in ethanol
464 (100%) (w/v) followed by the addition of 0.5 volume of hydrochloric acid (32%). The cortex of fixed

465 roots was removed. Desired segments were hand-cut from each root and mounted on glass slides using
466 freshly made staining solution. Slides were immediately observed and photographed with a Leica DM500
467 microscope equipped with an x40 objective and a Leica ICC50W camera (Leica, Germany).
468 *Estimation of the distance from root tip to the active silicification zone (ASZ)*
469 The distance of silica aggregates and lignin spots from the root tip was measured according to the tissue
470 autofluorescence (see (Zexer and Elbaum, 2020). The cortex of complete and fixed roots was removed.
471 The exposed stele of each root was cut to 1 cm long pieces, starting at the root tip, and keeping their
472 order up to the root basal end. Sections were then mounted on glass microscope slide using distilled
473 water. The autofluorescence pattern of blue spots (in Si+ roots, Soukup *et al.*, 2014) or green spots (in
474 Si- roots, (Zexer and Elbaum, 2020) was tracked from the basal section of the roots until no spots could
475 be identified. We recorded the length from the tip of each root to this section. Observations were
476 performed using a Nikon Eclipse 80i microscope (Nikon, Japan) and an X-cite 120Q (Lumen Dynamics,
477 Canada) UV light source. Specimens were observed using an x20 Nikon lens with the following set of
478 Nikon filters: GFP (excitation: 450–490 nm; emission: 500–550) and DAPI (excitation: 400–418 nm;
479 450–465 nm).
480 *Thermogravimetric analysis (TGA)*
481 Peeled primary roots were ground into fine powder using liquid nitrogen and a mortar and pestle (30
482 roots per sample). The crushed tissue was then dried at 65°C for at least 72 hours before use. Ground
483 and dried samples (16-20 mg) were mounted on platinum pans and measured using a Q500
484 thermogravimetric analyzer (TA instruments, USA). Pyrolysis was performed in a nitrogen atmosphere
485 and heating ramp of 15°C / min from room temperature up to 900°C. Calculation of the differential
486 thermal gravimetric (DTG) graphs was done using the Universal Analysis 2000 software (TA
487 instruments, USA). The relative quantification of the cell wall polymers was calculated by fitting peaks
488 to the DTG graphs and recording the area underneath the fitted decomposition peaks by WiRE3.2
489 software (Renishaw, New Mills, UK).
490 *Raman micro-spectroscopy*
491 Root segments were prepared as described for the aggregate assessments by SEM and mounted on
492 aluminum microscope slides using super glue. The samples were covered with a drop of double-distilled
493 water and measurements were made using an x63 water-immersed objective. Raman maps were collected
494 with a Renishaw InVia spectrometer equipped with a 532 nm laser (45 mW maximum intensity), utilizing
495 WiRE3.2 software (Renishaw, New Mills, UK). Measurements were performed by using the Streamline
496 mode with acquisition time of 30 sec. Maps were composed of between 3000 and 5000 spectra with steps

of 1 μm in the x direction. Spectral analysis was done in WiRE3.2 (Renishaw), including peak picking, first derivative calculation, and signal ratio mapping.

Statistics

Statistical analysis was preformed using the JMP statistical package version Pro15 (JMP®, SAS institute Inc., USA). Statistical significance was assumed at $p \leq 0.05$. For the comparisons of aggregates footprints area, in each treatment at least three roots were used and three micrographs from each root were analyzed (n = 600-1500 aggregates). For measurements of distances form the root tip to the ASZs, at least three roots per treatment were used. The data were subjected to ANOVA followed by the Tukey-Kramer post-Hoc test.

Acknowledgements

The research was funded by the Israeli Ministry of Agriculture & Rural Development, Chief Scientist Office grant 12-01-0016. N.Z is thankful to the Robert H. Smith Foundation for a scholarship.

511 ## References

512 **Abidi N, Hequet E, Cabrales L, Gannaway J, Wilkins T, Wells LW**. 2008. Evaluating cell wall structure and
513 composition of developing cotton fibers using Fourier transform infrared spectroscopy and thermogravimetric
514 analysis. Journal of Applied Polymer Science **107**, 476–486.

515 **Abraham Y, Dong Y, Aharoni A, Elbaum R**. 2018. Mapping of cell wall aromatic moieties and their effect on
516 hygroscopic movement in the awns of stork's bill. Cellulose **25**, 3827–3841.

517 **Agarwal UP**. 2014. 1064 nm FT-Raman spectroscopy for investigations of plant cell walls and other biomass
518 materials. Plant Biophysics and Modeling **5**, 490.

519 **Agarwal UP, Ralph SA**. 1997. FT-Raman Spectroscopy of Wood: Identifying Contributions of Lignin and
520 Carbohydrate Polymers in the Spectrum of Black Spruce (Picea mariana). Applied Spectroscopy **51**, 1648–1655.

521 **Barceló AR**. 1995. Peroxidase and not laccase is the enzyme responsible for cell wall lignification in the
522 secondary thickening of xylem vessels inLupinus. Protoplasma **186**, 41–44.

523 **Bennett DM**. 1982. An ultrastructural study on the development of silicified tissues in the leaf tip of barley
524 (*Hordeum sativum* jess). Annals of Botany **50**, 229–237.

525 **Casey WH, Kinrade SD, Knight CTG, Rains DW, Epstein E**. 2004. Aqueous silicate complexes in wheat, *Triticum*
526 *aestivum* L. Plant, Cell & Environment **27**, 51–54.

527 **Choudhury FK, Rivero RM, Blumwald E, Mittler R**. 2017. Reactive oxygen species, abiotic stress and stress
528 combination. The Plant Journal **90**, 856–867.

529 **Cooke J, Leishman MR**. 2016. Consistent alleviation of abiotic stress with silicon addition: a meta-analysis.
530 Functional Ecology **30**, 1340–1357.

531 **Coskun D, Deshmukh R, Sonah H, Menzies JG, Reynolds O, Ma JF, Kronzucker HJ, Bélanger RR**. 2019*a*. The
532 controversies of silicon's role in plant biology. New Phytologist **221**, 67–85.

533 **Coskun D, Deshmukh R, Sonah H, Menzies JG, Reynolds O, Ma JF, Kronzucker HJ, Bélanger RR**. 2019*b*. In
534 defence of the selective transport and role of silicon in plants. New Phytologist **223**, 514–516.

535 **Daudi A, O'Brien JA**. 2012. Detection of hydrogen peroxide by DAB staining in Arabidopsis leaves. Bio Protoc **2**,
536 1–4.

537 **Dixon RA, Barros J**. 2019. Lignin biosynthesis: old roads revisited and new roads explored. Open Biology **9**,
538 190215.

539 **Farhat W, Venditti R, Quick A, Taha M, Mignard N, Becquart F, Ayoub A**. 2017. Hemicellulose extraction and
540 characterization for applications in paper coatings and adhesives. Industrial Crops and Products **107**, 370–377.

541 **Fleck AT, Nye T, Repenning C, Stahl F, Zahn M, Schenk MK**. 2011. Silicon enhances suberization and
542 lignification in roots of rice (*Oryza sativa*). Journal of Experimental Botany **62**, 2001–2011.

543 **Frew A, Weston LA, Reynolds OL, Gurr GM**. 2018. The role of silicon in plant biology: a paradigm shift in
544 research approach. Annals of Botany.

545 **Fry SC, Willis SC, Paterson AEJ**. 2000. Intraprotoplasmic and wall-localised formation of arabinoxylan-bound
546 diferulates and larger ferulate coupling-products in maize cell-suspension cultures. Planta **211**, 679–692.

547 **Hatfield RD, Rancour DM, Marita JM**. 2017. Grass cell walls: A story of cross-linking. Frontiers in Plant Science
548 **7**, 2056.

549 **Hodson MJ**. 2016. The development of phytoliths in plants and its influence on their chemistry and isotopic
550 composition. Implications for palaeoecology and archaeology. Journal of Archaeological Science **68**, 62–69.

551 **Hoffmann N, Benske A, Betz H, Schuetz M, Samuels AL**. 2020. Laccases and Peroxidases Co-Localize in Lignified
552 Secondary Cell Walls throughout Stem Development. Plant Physiology **184**, 806–822.

553 **Kreszies T, Kreszies V, Ly F, Thangamani PD, Shellakkutti N, Schreiber L**. 2020. Suberized transport barriers in
554 plant roots: the effect of silicon. Journal of Experimental Botany.

555 **Kumar S, Adiram-Filiba N, Blum S, Sanchez-Lopez JA, Tzfadia O, Omid A, Volpin H, Heifetz Y, Goobes G,**
556 **Elbaum R**. 2020. Siliplant1 protein precipitates silica in sorghum silica cells (M Vaculik, Ed.). Journal of
557 Experimental Botany, eraa258.

558 **Kumar S, Elbaum R**. 2018. Interplay between silica deposition and viability during the life span of sorghum silica
559 cells. New Phytologist **217**, 1137–1145.

560 **Kumar S, Milstein Y, Brami Y, Elbaum M, Elbaum R**. 2017. Mechanism of silica deposition in sorghum silica
561 cells. New Phytologist **213**, 791–798.

562 **Lawton JR**. 1980. Observations on the structure of epidermal cells, particularly the cork and silica cells, from
563 the flowering stem internode of *Lolium temulentum* L. (Gramineae). Botanical Journal of the Linnean Society
564 **80**, 161–177.

565 **Lee Y, Rubio MC, Alassimone J, Geldner N**. 2013. A mechanism for localized lignin deposition in the
566 endodermis. Cell **153**, 402–412.

567 **Liang Y, Sun W, Zhu YG, Christie P**. 2007. Mechanisms of silicon-mediated alleviation of abiotic stresses in
568 higher plants: a review. Environmental Pollution **147**, 422–428.

569 **Lukačová Z, Švubová R, Kohanová J, Lux A**. 2013. Silicon mitigates the Cd toxicity in maize in relation to
570 cadmium translocation, cell distribution, antioxidant enzymes stimulation and enhanced endodermal
571 apoplasmic barrier development. Plant Growth Regulation **70**, 89–103.

572 **Lux A, Luxová M, Abe J, Tanimoto E, Hattori T, Inanaga S**. 2003. The dynamics of silicon deposition in the
573 sorghum root endodermis. New Phytologist **158**, 437–441.

574 **Meents MJ, Watanabe Y, Samuels AL**. 2018. The cell biology of secondary cell wall biosynthesis. Annals of
575 Botany **121**, 1107–1125.

576 **Mitani N, Ma JF, Iwashita T**. 2005. Identification of the silicon form in xylem sap of rice (*Oryza sativa* L.). Plant
577 and cell physiology **46**, 279.

578 **Mitani-Ueno N, Ma JF**. 2020. Linking transport system of silicon with its accumulation in different plant species.
579 Soil Science and Plant Nutrition **0**, 1–8.

580 **Prasad A, Sedlářová M, Balukova A, Rác M, Pospíšil P**. 2020. Reactive oxygen species as a response to
581 wounding: *In vivo* imaging in *Arabidopsis thaliana*. Frontiers in Plant Science **10**.

582 **Sakurai G, Satake A, Yamaji N, Mitani-Ueno N, Yokozawa M, Feugier FG, Ma JF**. 2015. In silico simulation
583 modeling reveals the importance of the Casparian strip for efficient silicon uptake in rice roots. Plant and Cell
584 Physiology **56**, 631–639.

585 **Sangster AG, Parry DW**. 1976. Endodermal silicon deposits and their linear distribution in developing roots of
586 *Sorghum bicolor* (L.) Moench. Annals of Botany **40**, 361–371.

587 **Sattler SE, Saathoff AJ, Haas EJ, Palmer NA, Funnell-Harris DL, Sarath G, Pedersen JF**. 2009. A Nonsense
588 Mutation in a Cinnamyl Alcohol Dehydrogenase Gene Is Responsible for the Sorghum brown midrib6
589 Phenotype. Plant Physiology **150**, 584–595.

590 **Schieber M, Chandel NS**. 2014. ROS function in redox signaling and oxidative stress. Current Biology **24**, R453–
591 R462.

592 **Schneider CA, Rasband WS, Eliceiri KW**. 2012. NIH Image to ImageJ: 25 years of image analysis. Nature
593 methods **9**, 671.

594 **Schuetz M, Benske A, Smith RA, Watanabe Y, Tobimatsu Y, Ralph J, Demura T, Ellis B, Samuels AL**. 2014.
595 Laccases direct lignification in the discrete secondary cell wall domains of protoxylem. Plant Physiology **166**,
596 798–807.

597 **Soukup M, Martinka M, Bosnić D, Čaplovičová M, Elbaum R, Lux A**. 2017. Formation of silica aggregates in
598 sorghum root endodermis is predetermined by cell wall architecture and development. Annals of Botany **120**,
599 739–753.

600 **Soukup M, Martinka M, Cigáň M, Ravaszová F, Lux A**. 2014. New method for visualization of silica phytoliths in
601 *Sorghum bicolor* roots by fluorescence microscopy revealed silicate concentration-dependent phytolith
602 formation. Planta **240**, 1365–1372.

603 **Soukup M, Rodriguez Zancajo VM, Kneipp J, Elbaum R**. 2020. Formation of root silica aggregates in sorghum is
604 an active process of the endodermis. Journal of Experimental Botany **71**, 6807–6817.

605 **Stewart D, Yahiaoui N, McDougall GJ, Myton K, Marque C, Boudet AM, Haigh J**. 1997. Fourier-transform
606 infrared and Raman spectroscopic evidence for the incorporation of cinnamaldehydes into the lignin of
607 transgenic tobacco (Nicotiana tabacum L.) plants with reduced expression of cinnamyl alcohol dehydrogenase.
608 Planta **201**, 311–318.

609 **Taylor LS, Zografi G**. 1997. Spectroscopic Characterization of Interactions Between PVP and Indomethacin in
610 Amorphous Molecular Dispersions. Pharmaceutical Research **14**, 1691–1698.

611 **Tobimatsu Y, Schuetz M**. 2019. Lignin polymerization: how do plants manage the chemistry so well? Current
612 Opinion in Biotechnology **56**, 75–81.

613 **Tsukagoshi H, Busch W, Benfey PN**. 2010. Transcriptional Regulation of ROS Controls Transition from
614 Proliferation to Differentiation in the Root. Cell **143**, 606–616.

615 **Van Bockhaven J, Vleesschauwer DD, Höfte M**. 2013. Towards establishing broad-spectrum disease resistance
616 in plants: silicon leads the way. Journal of Experimental Botany **64**, 1281–1293.

617 **Wang Y, Chantreau M, Sibout R, Hawkins S**. 2013. Plant cell wall lignification and monolignol metabolism.
618 Plant Biotechnology **4**, 220.

619 **Yahiaoui N, Marque C, Myton KE, Negrel J, Boudet AM**. 1997. Impact of different levels of cinnamyl alcohol
620 dehydrogenase down-regulation on lignins of transgenic tobacco plants. Planta **204**, 8–15.

621 **Yang H, Yan R, Chen H, Lee DH, Zheng C**. 2007. Characteristics of hemicellulose, cellulose and lignin pyrolysis.
622 Fuel **86**, 1781–1788.

623 **Zexer N, Elbaum R**. 2020. Unique lignin modifications pattern the nucleation of silica in sorghum endodermis.
624 Journal of Experimental Botany **71**, 6818–6829.

625